

## Transport properties and magnetic interactions in acceptor-type magnetic graphite intercalation compounds

N.-C. Yeh,\* K. Sugihara,<sup>†</sup> and M. S. Dresselhaus

*Department of Physics and Center for Materials Science and Engineering,  
Massachusetts Institute of Technology, Cambridge, Massachusetts 02139*

G. Dresselhaus

*Francis Bitter National Magnet Laboratory, Massachusetts Institute of Technology, Cambridge, Massachusetts 02139*

(Received 6 June 1988; revised manuscript received 9 December 1988)

Results on the resistivity of stage-1 and stage-2  $\text{CoCl}_2$  graphite intercalation compounds (GIC's) as a function of temperature ( $T$ ) and magnetic field ( $H$ ) are reported. The anomalies observed in the resistivity measurements at the magnetic phase transitions are explained by an interaction based on  $\pi$ - $d$  electron coupling. The contrasts in the  $T$  and  $H$  dependences of the resistivity between the stage-1 and stage-2 compounds for  $T < T_{cl}$  and  $H < H_{c2}$  are attributed to the different correlation lengths in the  $c$ -axis antiferromagnetic ordering. The magnitude of the interplanar antiferromagnetic coupling constant ( $J'$ ) in stage-1  $\text{CoCl}_2$  GIC's and the  $\pi$ - $d$  exchange coupling constant ( $J_{\pi-d}$ ) are estimated from the transport measurements. Magnetic exchange mechanisms are proposed by considering the relative contributions of the superexchange, dipole-dipole, and Ruderman-Kittel-Kasuya-Yosida (RKKY) interactions. We conclude that the superexchange interaction is the dominant magnetic interplanar coupling mechanism in pristine  $\text{CoCl}_2$  and stage-1  $\text{CoCl}_2$  GIC's, and is of comparable importance to the dipole-dipole interaction in stage-2 compounds. The dipole-dipole interaction is the dominant mechanism in higher stage GIC's ( $n \geq 3$ ). The RKKY interaction is always found to be negligibly small, due to the quasi-two-dimensional electronic properties of these acceptor GIC's.

### I. INTRODUCTION

The magnetic properties of transition-metal chloride graphite intercalation compounds (GIC's) have attracted extensive study, because the magnetic anisotropy in layered transition-metal chlorides is greatly enhanced by the insertion of nonmagnetic graphite layers, thereby providing an ideal environment for studying low-dimensional magnetic phase transitions.

The in-plane structure and magnetic interactions of the intercalants in the transition-metal chloride graphite intercalation compounds are nearly unchanged compared to their pristine form, while the interplanar repeat distance is enlarged by the presence of graphite layers. Therefore, systematic studies of three-dimensional (3D) to two-dimensional (2D) magnetic phase transitions become possible by controlling the number of graphite layers between consecutive magnetic layers. Special interest has been focused on  $\text{CoCl}_2$  GIC's and  $\text{NiCl}_2$  GIC's, because the strong  $XY$  anisotropy in the pristine chlorides<sup>1</sup> should make it possible to study the 2D Kosterlitz-Thouless transition<sup>2</sup> in these GIC's. Most of the experimental studies of their magnetic properties have been focused on neutron scattering,<sup>3-5</sup> magnetization,<sup>3,6</sup> magnetic-susceptibility,<sup>7,8</sup> and electron-spin-resonance<sup>9,10</sup> measurements.

Although the magnetic properties of the  $\text{CoCl}_2$  and  $\text{NiCl}_2$  GIC's have been extensively studied, the mechanism for the interplanar spin coupling between the magnetic layers through the nonmagnetic graphene layers has not yet been established. The exchange coupling mechanism in the pristine transition-metal chlorides is dominated

by the superexchange interaction. In the case of magnetic GIC's, the presence of conduction  $\pi$  electrons associated with the carbon layers complicates the interplanar superexchange interaction. In the limit of high-stage compounds, the superexchange interaction should become negligible so that only the long-range dipole-dipole interaction is important. Another possible mechanism for the interplanar magnetic coupling is an anisotropic Ruderman-Kittel-Kasuya-Yosida (RKKY) interaction,<sup>11-13</sup> associated with the layered distributions of the  $\pi$  conduction electrons and of the magnetic intercalate species. By studying the transport properties of acceptor-type magnetic GIC's, one can probe the  $\pi$ - $d$  electron exchange interaction, study the magnetic scattering effects in various magnetic phases, and explore the magnetic exchange mechanisms responsible for the interplanar coupling of magnetic GIC's.

In this paper, experimental results for the transport properties of magnetic  $\text{CoCl}_2$  GIC's are presented. In particular, large differences in the temperature ( $T$ ) and magnetic-field ( $H$ ) dependence of the resistivity between stage-1 and stage-2  $\text{CoCl}_2$  GIC's are reported and are attributed to a competition between two magnetic scattering effects. One is the typical spin-disorder scattering effect present in magnetic systems. The other is due to an additional scattering mechanism resulting from a modified Fermi surface, which is a consequence of the long-range  $c$ -axis antiferromagnetic ordering for  $T < T_{cl}$ , where  $T_{cl}$  is the 3D magnetic ordering temperature. The doubled  $c$ -axis magnetic periodicity in the antiferromagnetic phase extends the screening length for charged im-

purities of the system, thereby enhancing the charged-impurity scattering for  $T < T_{cl}$ .

The advantage of studying  $\text{CoCl}_2$  GIC's (relative to other intercalation compounds) is the strong in-plane ferromagnetic coupling ( $J = 28.5$  K) in pristine  $\text{CoCl}_2$  (Ref. 1) and the relatively weak interplanar antiferromagnetic coupling ( $J' = -2.16$  K) in pristine  $\text{CoCl}_2$  (Ref. 1) which simplify the theoretical analysis of the experimental data. At low temperatures where the ferromagnetic planar spin arrays can be approximated by a sheet of correlated spins (called "superpins"), a one-dimensional line of superpins<sup>8</sup> has been used to study the magnetic interactions. Since the transport studies in  $\text{CoCl}_2$  GIC's are sensitive only to the spatial low dimensionality of this system, not to the spin low dimensionality,<sup>3,4</sup> these transport measurements are not useful for examining special functional forms associated with Kosterlitz-Thouless-type phase transitions.

In this paper, the  $c$ -axis magnetic exchange mechanisms are discussed in terms of three types of interactions and their stage dependence: (1) a  $c$ -axis superexchange interaction through metal-insulator layers; (2) a RKKY interaction modified to treat a quasi-two-dimensional electronic system; and (3) the dipole-dipole interaction. It is concluded from this work that the superexchange interaction is the dominant  $c$ -axis magnetic coupling mechanism for both pristine  $\text{CoCl}_2$  and stage-1  $\text{CoCl}_2$  GIC's; this interaction decreases with increasing stage, becoming comparable to the dipole-dipole interaction in stage-2 samples. The dipole-dipole interaction becomes the dominant  $c$ -axis magnetic exchange mechanism for high-stage compounds ( $n \geq 3$ ). For all stages, the RKKY interaction is found to be negligibly small. Many aspects of the calculations for the magnetic exchange mechanisms given in this paper can be generalized to the whole class of transition-metal chloride GIC's.

## II. EXPERIMENTAL DETAILS

$\text{CoCl}_2$  GIC's were synthesized isothermally at  $560^\circ\text{C}$  for one month in pyrex glass ampoules.<sup>14</sup> The reaction ampoules contain the kish graphite host material, pristine  $\text{CoCl}_2$  powder, and  $\text{Cl}_2$  gas. Various stages can be obtained by varying the pressure of the  $\text{Cl}_2$  gas contained in the ampoules. A room-temperature chlorine gas pressure  $\geq 700$  torr was used for preparing stage-1  $\text{CoCl}_2$  GIC's, and  $\sim 500$  torr for stage 2. After the intercalation process was completed, the samples were taken out of the reaction ampoules and cleaned with diluted hydrochloric acid (HCl) to remove the residual pristine  $\text{CoCl}_2$  on the sample surfaces. The samples were then promptly dried and kept in airtight containers with desiccant to prevent moisture contamination.

The stage index and staging fidelity of the samples were characterized using (00l) x-ray diffraction. Samples used for these transport measurements were all single-staged GIC's (to better than 90%) according to their x-ray spectra. The  $c$ -axis repeat distance is  $I_c = 9.45 \pm 0.03$  Å for stage-1 and  $I_c = 12.80 \pm 0.03$  Å for stage-2  $\text{CoCl}_2$  GIC's. A typical size of these kish graphite-based samples is  $\sim 4 \times 3 \times 0.3$  mm<sup>3</sup>. The in-plane resistivity in both stage-1 and stage-2 samples was measured as a function of tem-

perature ( $2.9 \text{ K} \leq T \leq 300 \text{ K}$ ) and magnetic field ( $0 \leq H \leq 1.2$  kOe). The geometry for these transverse magnetoresistance measurements is  $\mathbf{j}, \mathbf{H} \perp c$  axis (with  $\mathbf{j} \perp \mathbf{H}$ ), where  $\mathbf{j}$  is the current density and  $\mathbf{H}$  is the applied field.

A standard four-point probe method was used in these resistivity measurements.<sup>15</sup> The electric contacts were made with silver paint by placing electrodes uniformly along a thin strip across the whole sample thickness to assure uniform current injection through all the layers. Low dc currents were used to avoid sample heating and temperature gradients across the samples. Such gradients would reduce the accuracy of our measurements, especially near the magnetic phase transition temperature. Sensitivity is an important issue since magnetic scattering effects in acceptor-type magnetic GIC's are much smaller than the residual resistivity in GIC's. Typical dc voltage readings in these experiments were only a few  $\mu\text{V}$  at liquid-helium temperatures, and the desired resolution for the magnetic scattering effects had to be better than  $\sim 100$  nV. For these small signal measurements, we used Keithley 181 nanovoltmeters with slow rise times ( $t_r \geq 8$  sec) in the built-in low-pass filter. Data were acquired through an IEEE bus to a computer. The sampling time (typically 10–30 sec) between consecutive data points was chosen to be long compared with the rise time of the filter.

Samples were mounted on the sample probe assembly after placement of the electrodes. A carbon-glass resistor sensor built into the probe was used for temperature monitoring. The resolution of the temperature readings in our resistivity measurements was better than  $\pm 0.01$  K for  $2.9 \text{ K} \leq T \leq 12$  K, and was within  $\pm 0.1$  K for temperatures up to 20 K. Helium gas was used in the ampoule for heat exchange.

The resistivity measurements on  $\text{CoCl}_2$  GIC samples were carried out on three stage-1 and three stage-2 samples to assure the reproducibility of the results. Similar measurements were also done on pristine kish graphite and nonmagnetic GIC samples such as  $\text{AlCl}_3$  GIC's and  $\text{SbCl}_5$  GIC's, using the same setup. All these measurements indicate that the observed low temperature anomalies in  $\text{CoCl}_2$  GIC's are uniquely related to the magnetic scattering, in contrast to the temperature and field dependences observed in pristine graphite and nonmagnetic GIC's, which were in agreement with previous work.<sup>16</sup>

## III. EXPERIMENTAL RESULTS

### A. Temperature dependence at constant magnetic field

Figures 1(a) and 1(b) show plots of the in-plane resistivity ( $\rho$ ) versus temperature ( $T$ ) at various constant magnetic fields for a typical stage-1 and two stage-2  $\text{CoCl}_2$  GIC samples, respectively. We shall first discuss the zero-field traces in Figs. 1(a) and 1(b), which display the following characteristics.

(1) For  $[(T - T_{cl})/T_{cl}] \gg 1$ , both stage-1 and stage-2  $\text{CoCl}_2$  GIC's exhibit a temperature-dependent resistivity that is typical for nonmagnetic GIC's. The resistivity  $\rho(T)$  in this temperature range can be fit to a functional

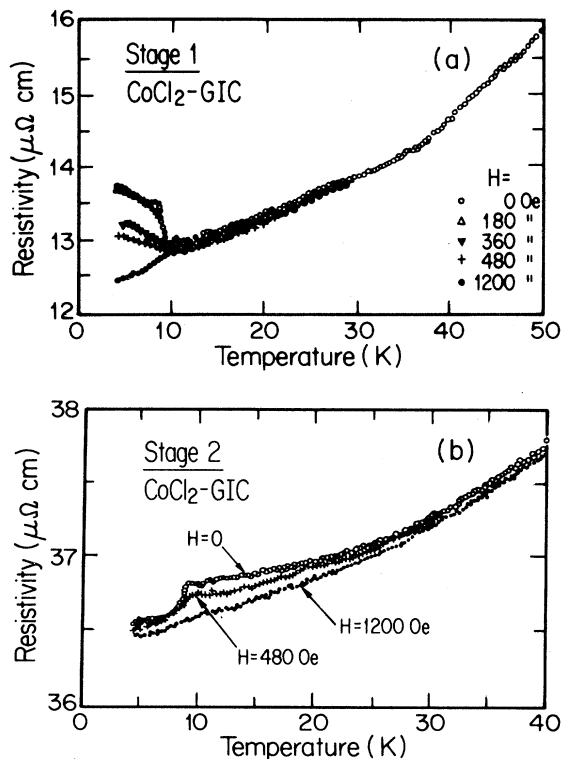


FIG. 1. Resistivity  $[\rho(H, T)]$  vs temperature ( $T$ ) for various constant magnetic fields: (a) stage-1  $\text{CoCl}_2$ -GIC's at  $H=0, 180, 360, 480,$  and  $1200$  Oe; (b) stage-2  $\text{CoCl}_2$ -GIC's at  $H=0, 480,$  and  $1200$  Oe. Above  $T_{cl}$  the resistivity of (a) is almost the same for all field values.

form<sup>16-18</sup>  $\rho(T) = A + BT + CT^2$ , where  $A$  represents the residual resistivity due to defect scattering, and the  $BT$  and  $CT^2$  terms in the temperature range  $T < 200$  K are related to the electron-phonon scattering from out-of-plane phonon vibrations,<sup>19</sup> while inter-pocket electron-phonon scattering plays an important role<sup>20</sup> for  $T > 200$  K. The resistivity coefficients,  $A$ ,  $B$ , and  $C$  are fit in the temperature range  $80 \text{ K} < T < 300 \text{ K}$ , where electron-phonon scattering is dominant, and the results are summarized in Table I, where it is seen that the coefficients  $A$ ,  $B$ , and  $C$  for these acceptor-type magnetic GIC's are

about 1 order of magnitude larger than those of nonmagnetic GIC's (Table I), but of similar magnitude to the  $A$ ,  $B$ , and  $C$  values observed in the magnetic donor-GIC  $\text{C}_6\text{Eu}$ .<sup>22</sup> The larger residual resistivity in the acceptor-type magnetic GIC's is attributed to a large concentration of structural defects and magnetic scattering effects present in these incommensurate acceptor GIC's.<sup>22-25</sup> However, the physical origin for the large electron-phonon scattering coefficients  $B$  and  $C$  remains unknown, but may be related to anomalies observed in recent magnetostriction experiments on stage-1  $\text{CoCl}_2$  GIC's.<sup>26,27</sup>

(2) As the temperature approaches the Néel temperature ( $T_N = T_{cl}$ ) from above, i.e., in the temperature range  $0 < [(T - T_{cl})/T_{cl}] < 1$ , the resistivity exhibits a weak temperature dependence. The resistivity in this temperature range can be fit to a functional form  $\rho(T) = A' + B'T$  where  $B' \ll B$ . This temperature dependence is characteristic of short-range spin ordering in typical magnetic systems,<sup>28</sup> as is discussed in Sec. IV.

(3) For  $T < T_{cl}$ , the stage-1 and stage-2 data exhibit fundamental differences with respect to the sign and magnitude of the change in the resistivity with temperature: i.e.,  $[d\rho(T)/dT]_{\text{stage-1}} < 0$  and  $[d\rho(T)/dT]_{\text{stage-2}} > 0$ . While the sharp decrease in the resistivity for  $0 < [(T_{cl} - T)/T_{cl}] < 1$  in stage-2  $\text{CoCl}_2$  GIC's is characteristic of resistivity anomalies associated with spin-disorder scattering in a magnetic system,<sup>28</sup> the behavior for stage-1 is anomalous insofar as the resistivity *increases* as  $T$  is lowered below  $T_{cl}$ , indicating an additional scattering effect. We attribute this additional scattering to the presence of long-range interplanar antiferromagnetic ordering<sup>29</sup> in the stage-1 compound, as discussed in Ref. 30. Note that the total *increase* in resistivity from  $T_{cl}$  to lower temperatures ( $T = 4.2 \text{ K}$ ) in the stage-1 compounds is about 10% of  $\rho(T = 4.2 \text{ K})$ , while the *decrease* in  $\rho(T)$  for stage-2 in the same temperature range is only about -1% of  $\rho(T = 4.2 \text{ K})$ . This indicates that the scattering effect associated with the antiferromagnetic ordering dominates over the spin-disorder scattering, thereby giving rise to an anomalous negative sign in  $[d\rho(T)/dT]$  for stage-1  $\text{CoCl}_2$  GIC's. In a separate paper we show how to extract information on the  $\pi$ - $d$  electron exchange coupling constant ( $J_{\pi-d}$ ) from the experimental resistivity data.<sup>30</sup>

TABLE I. Comparison of the in-plane resistivity coefficients  $A$ ,  $B$ , and  $C$  of the functional form  $\rho(T) = A + BT + CT^2$  for various GIC's. The resistivity coefficients of the magnetic GIC's are obtained by fitting the experimental data in the temperature range  $80 < T < 300 \text{ K}$ , where the magnetic scattering contribution can be treated as a constant.

Sample	Stage	$A$ ( $\mu\Omega \text{ cm}$ )	$B$ ( $\mu\Omega \text{ cm/K}$ )	$C$ ( $\mu\Omega \text{ cm/K}^2$ )
$\text{C}_8\text{K}^a$	1	1.86	$7.48 \times 10^{-3}$	$15.36 \times 10^{-5}$
$\text{C}_4\text{KH}_{0.8}^b$	1	0.18	$4.8 \times 10^{-3}$	$3.0 \times 10^{-5}$
$\text{C}_6\text{Eu}^c$	1	11.8	$110 \times 10^{-3}$	$6 \times 10^{-5}$
$\text{C}_{5.2}\text{CoCl}_{2.03}^b$	1	15	$65 \times 10^{-3}$	$53 \times 10^{-5}$
$\text{C}_{10.6}\text{CoCl}_{2.03}^b$	2	36	$59 \times 10^{-3}$	$11 \times 10^{-5}$

<sup>a</sup>Reference 18.

<sup>b</sup>Reference 21.

<sup>c</sup>Reference 22.

As shown in Figs. 1(a) and 1(b), the magnitudes of the anomalies in the resistivity for both stage-1 and stage-2  $\text{CoCl}_2$  GIC's gradually decrease with increasing external magnetic field for the geometry of the resistivity measurements  $\mathbf{j} \perp \mathbf{H}$ , and  $\mathbf{H} \perp c$  axis. In the case of stage 1, there is no observable field dependence for the resistivity  $[\rho(H, T)]$  in the temperature range  $T \ll T_{cl}$  and the magnetic-field range  $H < 300$  Oe [Fig. 1(a)], consistent with the magnetoresistance data, shown in the next subsection. As  $H$  is increased above 300 Oe, the magnitude of the temperature-dependent anomaly in  $\rho(H, T)$  in the range  $T < T_{cl}$  gradually decreases [Fig. 1(a)], and finally at yet higher fields the anomalous negative slope in  $d\rho(T)/dT$  disappears. The difference in the resistivity between  $H = 0$  and  $H = 1.2$  kOe is plotted as a function of  $T$  in Fig. 2(a), where it is seen that the magnitude of the negative magnetoresistance decreases by only a factor of 2 as  $T$  is increased between 2.9 K and 8.3 K, and then drops rapidly as  $T$  increases close to  $T_{cl}$ .

In contrast, the increase of the zero-field resistivity near  $T_{cl}$  due to the spin-disorder scattering in the stage-2 compound is gradually reduced as the external field increases [Fig. 1(b)]. The negative magnetoresistance versus  $T$  at

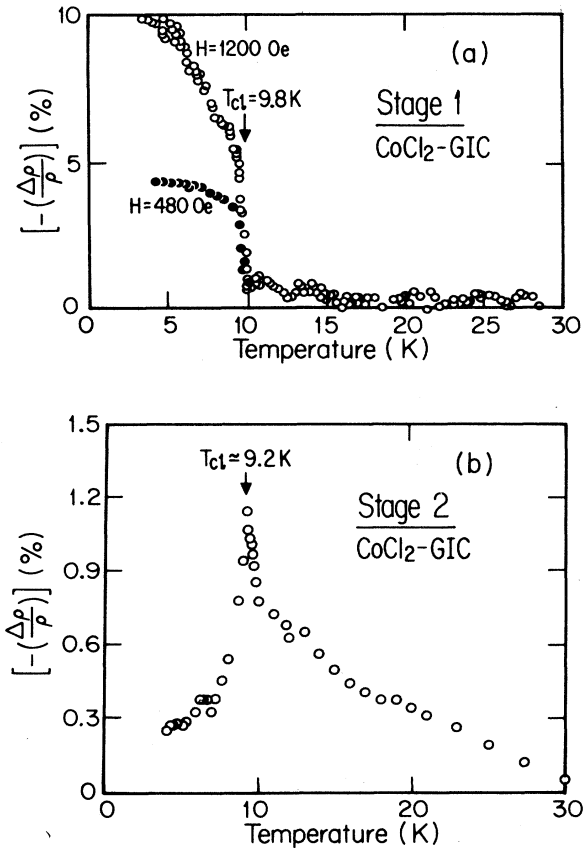


FIG. 2. Negative magnetoresistivity  $[-\Delta\rho/\rho(0, T)]$  vs temperature ( $T$ ) for (a) stage-1  $\text{CoCl}_2$  GIC's at  $H = 1200$  and 480 Oe; and (b) stage-2  $\text{CoCl}_2$  GIC's at  $H = 1200$  Oe. Here  $\Delta\rho \equiv \rho(H, T) - \rho(0, T)$ .

$H = 1.2$  kOe is shown in Fig. 2(b), where the negative magnetoresistance  $-(\Delta\rho/\rho)$  is defined in terms of  $\rho(H, T)$  as  $[\rho(0, T) - \rho(1.2 \text{ kOe}, T)]/\rho(0, 4.2 \text{ K})$ . For  $T \ll T_{cl}$ , inelastic neutron scattering measurements on stage-2 compounds<sup>4,5,31,32</sup> show that the spin system exhibits static magnetic ordering with a magnetic coherence distance along the  $c$  axis of about five unit cells. Therefore, the presence of an external magnetic field only has a small effect on suppressing the spin fluctuations, resulting in a small negative magnetoresistance. Furthermore, when  $T \gg T_{cl}$ , the scattering is dominated by the electron-phonon interaction, so that the external field also has little effect on suppressing the scattering. Only for  $T \simeq T_{cl}$ , where the spin system undergoes large thermal fluctuations, is the external field effective in greatly reducing the magnetic scattering (see Sec. IV), thereby accounting for the sharp peak at  $T_{cl}$  in the negative magnetoresistance in stage-2  $\text{CoCl}_2$  GIC's. The slow decrease of  $[-\Delta\rho/\rho]$  for  $T > T_{cl}$  is related to the short-range spin correlation, which contributes a weak temperature dependence to the resistivity. Strong short-range spin correlations have been proposed for the range  $T_{cl} < T < T_{cu}$  where the magnetic vortices bind in the Kosterlitz-Thouless state.<sup>33,34</sup> On the other hand, there is no observable anomaly of the resistivity in stage-2  $\text{CoCl}_2$  GIC's at the upper critical temperature  $T_{cu} = 10.3$  K, indicating that the transport measurements are not sensitive to a possible Kosterlitz-Thouless phase transition, in contrast to the magnetic-susceptibility measurements.<sup>35,36</sup>

### B. Field dependence at constant temperature

Figures 3(a) and 3(b) show magnetoresistance data for the geometry  $\mathbf{j}, \mathbf{H} \perp c$  axis and  $\mathbf{j} \perp \mathbf{H}$  at various constant temperatures for stage-1 and stage-2  $\text{CoCl}_2$  GIC's. We discuss the stage-2 data first because it is relatively simpler.

At all temperatures the resistivity data in Fig. 3(b) exhibit an approximately linear decrease with increasing  $H$  in the small magnetic field range (i.e.,  $-\{d\rho/dH\} \approx \text{const}$  for  $g^* \mu_B S H \ll k_B T$ , where  $g^*$  is the effective  $g$  value), and then saturation behavior at higher magnetic fields  $[-\{d\rho/dH\} \sim 0$  for  $(g^* \mu_B S H) \gg k_B T]$ . This  $H$  dependence is typical for spin-disorder scattering, where the resistivity has the functional form<sup>21,25</sup>

$$\rho(H, T) = \rho(0, T) \left[ 1 - \frac{S B_S(x)}{S(S+1)} \right]. \quad (1)$$

Here  $x \equiv [g^* \mu_B S H_{\text{eff}}/k_B(T - \Theta)]$ , where  $g^*$  is the effective  $g$  value, and  $B_S(x)$  is the Brillouin function, which has the functional form  $B_S(x) \propto x$  for  $x \ll 1$  and  $B_S(x) \rightarrow 1$  for  $x \gg 1$ . The Curie-Weiss temperature  $\Theta$  has been shown, from the high-temperature magnetic-susceptibility data of  $\text{CoCl}_2$  GIC's,<sup>35</sup> to be a small number (i.e.,  $\Theta < 1$  K). Therefore in the following discussion we simplify the parameter  $x$  by writing  $x = (g^* \mu_B S H_{\text{eff}}/k_B T)$ . The effective field ( $H_{\text{eff}}$ ) for  $T < T_{cl}$  is the sum of the applied field ( $H$ ) and the exchange field ( $H_E$ ). Thus for  $T < T_{cl}$ , the magnetoresistance approaches zero (saturation behavior sets in) even for a small external field,

provided that  $H > H_E$  [see Fig. 3(b), traces A–D]. In contrast, the effective field for  $T > T_{cl}$  is equal to the applied field and therefore the magnetoresistance shows a linear decrease with  $H$  over the entire field range  $H \leq 1.2$  kOe [see Fig. 3(b), traces E, F]. Thus, both the temperature and magnetic-field dependence of the resistivity provide support for the spin-disorder scattering effect in the stage-2 compounds. (See next section.)

The total decrease of  $\rho(H, T)$  from  $H = 0$  to  $H = 1.2$  kOe is nearly constant for  $T \ll T_{cl}$  [see Fig. 3(b), traces A–D], the magnitude of the negative magnetoresistance for  $T \ll T_{cl} \approx 9.2$  K being about

$$\frac{\rho(1.2 \text{ kOe}, T) - \rho(0, T)}{\rho(0, 4.2 \text{ K})} < -0.5\% , \quad (2)$$

and increasing rapidly to  $\sim -1.2\%$  for  $T \sim T_{cl}$  as shown in Fig. 2(b).

In the case of the stage-1 data [Fig. 3(a)], the  $H$  dependence for the trace with  $T > T_{cl}$  [Fig. 3(a), trace E] shows

similar behavior as was seen in the stage-2 data, indicating a decrease in the spin-disorder scattering with increasing magnetic field for  $T > T_{cl} \approx 9.8$  K. However, for  $T < T_{cl}$ , anomalous contrasts to the stage-2 behavior are observed. Firstly, for each constant temperature trace, the resistivity is nearly constant up to a critical field  $H_{c2}(T)$  (e.g.,  $H_{c2} \approx 330$  Oe for  $T = 4.2$  K), above which a rapid decrease of resistivity takes place to about 550 Oe, and only a very weak  $H$  dependence is observed for  $H > 600$  Oe. Secondly, the  $H_{c2}$  values are found to be nearly temperature independent for  $T$  well below  $T_{cl}$ , and to decrease as  $T$  increases to  $T_{cl}$  from below. If we plot  $H_{c2}$  versus  $T$  [inset in Fig. 3(a)], the data points are in good agreement with the  $H_{c2}(T)$  curve on the magnetic phase diagram obtained from the magnetic susceptibility measurements.<sup>35,36</sup> The  $H_{c2}(T)$  curve observed from the transport measurements corresponds to the phase transition identified from the susceptibility measurements<sup>35,36</sup> and the Monte Carlo simulations with the loss of antiferromagnetic interplanar coupling between the superspins. The transport measurements do not give a definitive identification of the magnetic phases at the magnetic phase boundary, as will be discussed. Thirdly, as already noted, the magnitude of the negative magnetoresistance for  $T \ll T_{cl}$  is about one order of magnitude larger than that in stage 2, i.e.,

$$\frac{\rho(1.2 \text{ kOe}, T) - \rho(0, T)}{\rho(0, 4.2 \text{ K})} \sim -10\% \quad (3)$$

for  $T = 4.2$  K. The magnitude of the negative magnetoresistance defined by the left-hand side of Eq. (3) decreases gradually with increasing temperature, and then drops rapidly as  $T$  approaches  $T_{cl}$  from below. The magnetoresistance ranges from  $\sim -10\%$  at  $T = 4.2$  K to  $\sim -1.5\%$  at  $T \approx T_{cl} \approx 9.8$  K, consistent with Fig. 2(a).

These features imply a second scattering effect for the  $\pi$ -conduction electrons in the stage-1 compounds below  $T_{cl}$  in addition to the spin-disorder scattering which dominates the stage-2 behavior. Specifically, we identify the second scattering effect with the antiferromagnetic interplanar ordering below  $T_{cl}$ , and the experimental results [Figs. 2(a) and 3(a)] show that the second scattering effect dominates over the spin-disorder scattering effect in the stage-1 compounds.

#### IV. THEORETICAL MODELING

In this section, we begin with a general description of the temperature dependence of the resistivity associated with the magnetic scattering of  $\pi$ -conduction electrons in zero magnetic field. We focus on the physical meanings of the temperature-dependent resistivity in various temperature regions. The detailed calculations for the zero-field temperature dependence of the resistivity are presented in a separate paper.<sup>30</sup> We focus here on the phenomenological calculations for the magnetic-field dependence, compare the effects of varying  $T$  and  $H$ , and

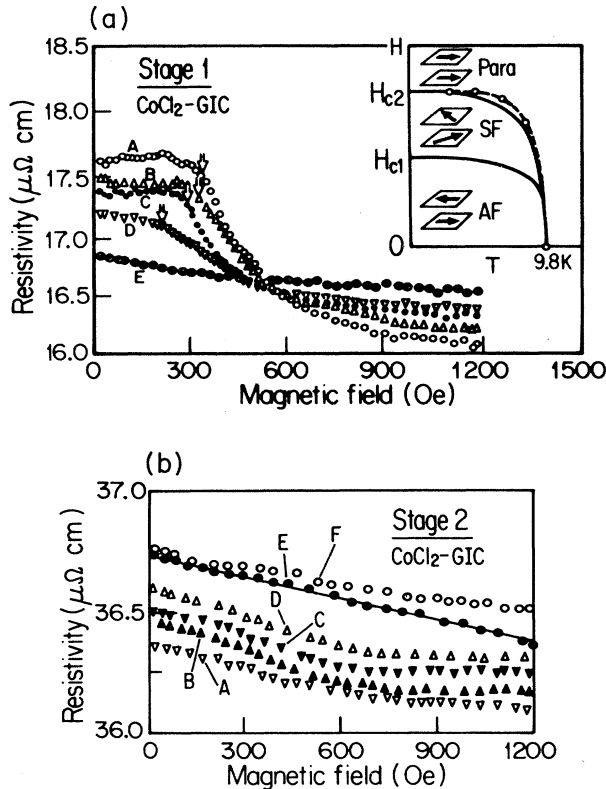


FIG. 3. Resistivity [ $\rho(H, T)$ ] vs magnetic field ( $H$ ) data (points) at various constant temperatures: (a) Stage-1  $\text{CoCl}_2$  GIC's at  $T =$ : (A) 4.2 K, (B) 6.0 K, (C) 8.0 K, (D) 9.0 K, and (E) 10.0 K  $\geq T_{cl} = 9.8$  K. The inset is the magnetic phase diagram obtained from magnetic susceptibility (lines) and resistivity (points) measurements.<sup>8,35,36</sup> The critical fields (arrows) obtained from these data were chosen at the fields where 10% of the total decrease in the resistivity took place. (b) Stage-2  $\text{CoCl}_2$  GIC's at  $T =$ : (A) 4.2 K, (B) 6.0 K, (C) 7.8 K, (D) 8.5 K, (E) 9.4 K  $\geq T_{cl} \approx 9.2$  K, and (F) 10.5 K  $\geq T_{cu} \approx 9.4$  K.

summarize the consistency between the experimental data and our theoretical calculations.

### A. General description

The basic concept in calculating the magnetic scattering is the exchange coupling between the  $\pi$  conduction electrons and the magnetic  $d$  electrons of the cobalt ions. This is reminiscent of the  $s$ - $d$  electron exchange coupling in magnetic alloys, except that in  $\text{CoCl}_2$  GIC's, the  $\pi$  and  $d$  electrons are separated by chlorine layers. Therefore an explicit expression for the  $\pi$ - $d$  exchange interaction has to include the effect of the intervening chlorine wave functions. In the following calculations, we shall treat the coupling constant  $J_{\pi-d}$  as an empirical constant determined from experiments. The quantity  $J_{\pi-d}$  is calculated in a separate paper<sup>30</sup> in terms of a microscopic picture of the  $\pi$  electron,  $\text{Co}^{2+}$  and  $\text{Cl}^-$  wave functions.

For a one-carrier metallic system, which is a reasonable assumption for low-staged GIC's, each component of the total resistivity tensor ( $\rho_{\text{total}}$ ) can be written as

$$(\rho_{\text{total}})_{ij} = \frac{m_{ij}^*}{ne^2} \sum_s \frac{1}{\tau_s}, \quad i, j = x, y, z, \quad (4)$$

where  $\tau_s$  is the relaxation time of the  $s$ th scattering mechanism for the  $ij$  component,  $m_{ij}^*$  is the effective mass of the carriers at the Fermi level, and  $n$  is the carrier density.

In magnetic GIC's, we can assume an "easy-plane" anisotropy; i.e.,  $m_{xx}^* = m_{yy}^* \neq m_{zz}^*$  and  $(1/\tau)_{xx} = (1/\tau)_{yy}$ . Since we focus here on the in-plane resistivity, Eq. (4) is written

$$\rho_{\text{total}} = \frac{m_{ab}^*}{ne^2} \sum_s \frac{1}{\tau_s}, \quad (5)$$

and the anisotropy effects are incorporated in the scattering matrix elements which determine the scattering rate due to each scattering mechanism. More specifically, the resistivity can be generally written as a combination of several scattering processes:

$$\rho_{\text{total}} = \rho_0 + \rho_{e\text{-ph}} + \rho_{\text{spin}}, \quad (6)$$

where  $\rho_0$  is the temperature-independent resistivity which includes the Coulomb impurity scattering contribution  $\rho_I$  and the residual resistivity due to other defects ( $\rho_r$ ), where  $\rho_0 = \rho_I + \rho_r$ . Here  $\rho_{e\text{-ph}}$  is the resistivity from electron-phonon scattering, which includes both the intrapocket scattering which is proportional to  $T$ , and the inter-pocket scattering which is proportional to  $T^2$  in GIC's.<sup>20</sup> Finally  $\rho_{\text{spin}}$  is the magnetic scattering term. Each term in Eq. (6) is highly anisotropic. Normally in isotropic magnetic systems such as magnetic alloys, the only source of magnetic scattering comes from spin-disorder scattering  $\rho_{\text{spin}}$ . However, in the highly anisotropic stage-1  $\text{CoCl}_2$  GIC, there is an additional scattering contribution associated with an increase of the charged-impurity scattering arising from the antiferromagnetic ordering of the ferromagnetically ordered planes of spins.<sup>21,30</sup> It was shown<sup>30</sup> that the long-range  $c$ -

axis antiferromagnetic ordering of these planes of spins in stage-1  $\text{CoCl}_2$  GIC's for  $T < T_{cl}$  results in a zone-folding effect in reciprocal space, thereby splitting the original  $c$ -axis dispersion relation into two bands, modifying the wave functions and scattering matrix elements and enhancing the resistivity  $\rho_I$ , for both the in-plane and  $c$ -axis components of the resistivity.

In the following discussion we consider the  $\pi$ - $d$  exchange interaction as the dominant mechanism for the in-plane resistivity anomalies in  $\text{CoCl}_2$  GIC's. The  $\pi$ - $d$  exchange interaction is decomposed into two contributions:<sup>21,30</sup>

$$\begin{aligned} \mathcal{H}_{\pi-d}(\mathbf{r}) &= \mathcal{H}_{\pi-d}^{(1)} + \mathcal{H}_{\pi-d}^{(2)}, \\ &= -\frac{J_{\pi-d}(0)}{N_0} \sum_n \sum_{\mathbf{k}} \langle \mathbf{k} | \sigma | \mathbf{k} \rangle \langle \mathbf{S}_n \rangle \\ &\quad - \frac{1}{N_0} \sum_n \sum_{\mathbf{k}, \mathbf{k}'} e^{i(\mathbf{k}-\mathbf{k}') \cdot \mathbf{R}_n} J_{\pi-d}(\mathbf{k}-\mathbf{k}') \\ &\quad \times \langle \mathbf{k} | \sigma | \mathbf{k}' \rangle \{ \mathbf{S}_n - \langle \mathbf{S}_n \rangle \}. \quad (7) \end{aligned}$$

Here  $\langle \mathbf{S}_n \rangle$  is the thermodynamic average of the spin angular momentum, and  $N_0$  is the number of unit cells per unit volume. The first term  $\mathcal{H}_{\pi-d}^{(1)}$  in Eq. (7) is associated with an additional periodicity due to the  $c$ -axis antiferromagnetic ordering, which results in a perturbation in the  $c$ -axis energy dispersion relation.<sup>30</sup> The second term  $\mathcal{H}_{\pi-d}^{(2)}$  in Eq. (7) is related to the thermal fluctuation of the spins ( $\mathbf{S}_n - \langle \mathbf{S}_n \rangle$ ), which is the origin of the spin-disorder scattering.

### B. Spin-disorder scattering

Since the  $c$ -axis correlation length for the antiferromagnetic alignment of the ferromagnetic sheets of spins does not exceed several  $c$ -axis repeat distances  $I_c$  in stage-2  $\text{CoCl}_2$  GIC's, the dominant magnetic scattering effect in the stage-2 compounds comes from the spin-disorder scattering. The scattering rate due to spin fluctuations is evaluated by using  $\mathcal{H}_{\pi-d}^{(2)}$  from Eq. (7), and the final result can be written as a sum of the autocorrelation and distinct spin-correlation terms.<sup>30</sup> In this section, we first give the derived analytical forms and the physical meanings of these two contributions, and then show the agreement between the modeling and the experimental data.

The scattering rate due to the spin-disorder scattering can be written<sup>30</sup>

$$\begin{aligned} \frac{1}{\tau_{\text{spin}}(E_F)} &= \frac{2J_{\pi-d}^2}{\hbar} \left[ \frac{\Omega}{N_0} \right] \left[ \frac{N_s}{N_0} \right] \mathcal{N}(E_F) \\ &\quad \times \left[ \frac{\pi}{4} \Gamma(0) + \frac{1}{2} \sum_{n \neq 0} \Gamma(\mathbf{R}_n, T) F(R_n) \right], \quad (8) \end{aligned}$$

where  $\Omega$  is the volume of the sample,  $\mathbf{R}_n$  is a lattice vector,  $F(R_n)$  is a fast oscillatory function of  $k_F R_n$  (Ref. 30) resembling the Friedel oscillation:

$$F(R_n) \simeq \left[ \frac{2}{\pi} \right]^{1/2} \frac{\sin(2k_F R_n - \pi/4)}{(2k_F R_n)^{3/2}} + \frac{3}{(2\pi)^{1/2}} \frac{\cos(2k_F R_n - \pi/4)}{(2k_F R_n)^{5/2}} - \frac{1}{(2k_F R_n)^3}, \quad (9)$$

and  $\Gamma(\mathbf{R}_n, T)$  is the spin-spin correlation function which is defined as

$$\Gamma(\mathbf{R}_n, T) \equiv \langle \{S_0 - \langle S_0 \rangle\} \cdot \{S_n - \langle S_n \rangle\} \rangle \text{ for } R_n \neq 0. \quad (10)$$

Since  $\Gamma(\mathbf{R}, T)$  is proportional to the imaginary part of the magnetic susceptibility<sup>37</sup> which is directly related to the energy dissipation, the appearance of  $\Gamma(\mathbf{R}_n, T)$  in the scattering rate is expected. We now discuss the physical meanings of the autocorrelation function  $\Gamma(0)$  and the distinct spin-correlation contribution  $\sum_{n \neq 0} \Gamma(\mathbf{R}_n, T)F(R_n)$  of Eq. (8), and then give an estimate of the temperature dependence of each of the contributions to the in-plane resistivity.

The first contribution that we consider is the autocorrelation function  $\Gamma(0)$  which is not given by  $\langle (S - \langle S \rangle)^2 \rangle$ , but rather by

$$\Gamma(0) = \langle \mathbf{S} \cdot \mathbf{S} \rangle - \langle S_z \rangle^2 \equiv S^2 + \Gamma(0, T), \quad (11)$$

$$\Gamma(0, T) = S - \langle S_z \rangle \propto M_0 \left[ 1 - \left\{ \frac{M_s(T)}{M_0} \right\} \right],$$

where  $M_0 = \frac{1}{2} N_s g^* \mu_B S$  is the saturated sublattice magnetization at  $T=0$ , and the sublattice magnetization  $M_s(T)$  obeys the functional form  $M_s(T) = M_0 [1 - (T/T_{cl})]^\beta$  for  $T < T_{cl}$  (here  $\beta$  represents a positive universal exponent<sup>38</sup>). Also,  $M_s(T > T_{cl}) = 0$  because of the breakdown of long-range spin-ordering. Thus, the scattering rate associated with  $\Gamma(0, T)$  is nearly zero for  $T \ll T_{cl}$ . The corresponding resistivity then increases with increasing  $T$  according to the functional form

$$\rho(T \rightarrow T_{cl}) = \rho_s \{ 1 - [1 - (T/T_{cl})]^\beta \},$$

and finally saturates at a constant value  $\rho_s$ , since according to Eq. (11),  $\Gamma(0, T_{cl}) = S$ . The contribution to the temperature-dependent resistivity from the autocorrelation function  $\Gamma(0)$  thus obtained is plotted in Fig. 4(a).

The second term in Eq. (8) is related to the short-range spin correlation by the following considerations. The sum over all the spins  $\sum_{n \neq 0} \Gamma(\mathbf{R}_n, T)F(R_n)$  only has an important contribution from the range near  $R_n \sim \min(\xi, l_0, 1/2k_F)$ , where  $\min(x, y, z)$  refers to the smallest value among  $x, y, z$ . The magnitude of this contribution to the scattering rate can be estimated by a phenomenological formula<sup>38</sup>

$$\Gamma(\mathbf{R}, T) = A \frac{e^{-R/\xi}}{R}, \quad (12)$$

where the correlation length is written as  $\xi(T) \propto |T - T_{cl}|^{-\nu}$ , in which  $\nu$  is a positive universal exponent.<sup>38</sup> The contribution to the temperature-dependent resistivity from the distinct spin correlation function  $\sum_{n \neq 0} \Gamma(\mathbf{R}_n, T)F(R_n)$  is shown in Fig. 4(b). In obtaining this result, we have considered lattice vectors  $R_n$  only up

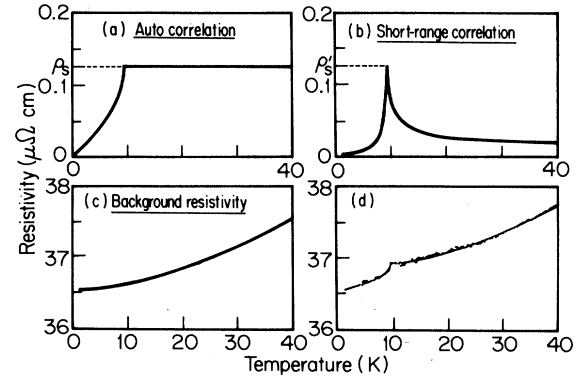


FIG. 4. Theoretical plots of the contribution to the temperature dependence of the resistivity from (a) the autocorrelation function  $\Gamma(0)$ ; (b) the contribution to the resistivity from the distinct-spin contribution  $\sum_{n \neq 0} \Gamma(\mathbf{R}_n, T)F(R_n)$ ; (c) the best fit of the background resistivity using the functional form  $\rho(T) = A + BT + CT^2$ ; and (d) theoretical and experimental plots of  $\rho(T)$  vs temperature. The solid line is a fit based on the sum of the contributions from (a)–(c). The points are the experimental data (see text).

to the second-nearest neighbors. This simplification does not lead to any substantial error because of the exponential decrease of  $\Gamma(\mathbf{R}_n, T)$  as well as the power-law decrease and oscillatory spatial dependence of  $F(R_n)$  as  $R_n$  increases. Figure 4(b) shows that the distinct spin-correlation term has a maximal value of  $\rho'_s$  at  $T_{cl}$ , and decreases monotonically as the temperature deviates from  $T_{cl}$ . It is also seen that  $\rho'_s$  in Fig. 4(b) is of the same order of magnitude as  $\Gamma(0, T_{cl})$  in Fig. 4(a).

The large background resistivity shown in Fig. 4(c) is a combination of the electron-phonon scattering term and the residual resistivity due to the impurity scattering, and is fit to the experimental results for  $T \gg T_{cl}$ . The total resistivity, which is the sum of the autocorrelation, short-range correlation, and the electron-phonon interaction [plotted in Fig. 4(d)], results in a weak temperature dependence in the magnetically ordered phase, a sharp increase in the resistivity for  $T \rightarrow T_{cl}$  from below, a weak temperature dependence in the temperature range  $0 < (T - T_{cl})/T_{cl} \ll 1$ , and a typical electron-phonon scattering behavior for  $T \gg T_{cl}$ . The agreement between the numerical calculations and the experimental data points in Fig. 4(d) indicates that the transport anomaly at  $T_{cl}$  for the stage-2 compounds is associated with spin-disorder scattering, and the results are typical of spin-disorder scattering observed in magnetic metallic systems.<sup>28</sup> The exponents  $\beta$  and  $\nu$  are found from the fits in Figs. 4(a) and 4(b), yielding  $\beta = 0.46$  and  $\nu = 0.5$ ; the value  $\nu = 0.5$  corresponds to the Ginsberg-Landau mean-field theory.<sup>38</sup>

It is shown by Sugihara *et al.*<sup>30</sup> that the  $\pi$ - $d$  exchange coupling constant  $J_{\pi-d}$  can be estimated from Eqs. (4) and (8) in comparison with the observed result for  $\Delta\rho = \rho(4.2 \text{ K}) - \rho(T_{cl})$ , where

$$\Gamma(0, T_{cl}) = \frac{2}{\pi} \sum_{n \neq 0} \Gamma(\mathbf{R}_n, T_{cl})F(R_n) \quad (13)$$

is assumed.<sup>30</sup> In this comparison, the value of  $J_{\pi-d}$  for stage-2  $\text{CoCl}_2$  GIC's is estimated to be  $\sim 5 \times 10^{-2}$  eV, and this value was used in the numerical estimates of Fig. 4. It is of significance that  $J_{\pi-d}$  for stage-2  $\text{CoCl}_2$  GIC's is approximately 1 order of magnitude smaller than the  $J_{\pi-f}$  value in  $\text{C}_6\text{Eu}$ .<sup>22,23,24</sup> This is consistent with the relatively larger spatial separation between the  $\pi$  and  $d$  electrons in the case of stage-2  $\text{CoCl}_2$  GIC's (i.e., 4.71 Å) as compared with the  $\pi-f$  separation of 2.43 Å in  $\text{C}_6\text{Eu}$ . However, the estimate for  $J_{\pi-d}$  must be considered very approximate since several untested approximations and simplifications are employed in estimating  $J_{\pi-d}$ .

### C. Fermi-surface modification effect

As shown in Eq. (7), the  $\pi-d$  exchange interaction results in two effects on the conduction-electron scattering. One is the spin-disorder scattering, which has been discussed in the previous subsection. The other is a Fermi-surface modification effect which becomes dominant for the stage-1  $\text{CoCl}_2$  GIC because of the additional magnetic periodicity of this compound along the  $c$  axis. Detailed mathematical calculations for this scattering effect are provided elsewhere.<sup>30</sup> Here we only comment on the physical significance of this effect.

Typically for a metallic system at very low temperature, the electron-phonon scattering is so weak that the dominant scattering comes from the impurity scattering ( $\rho_0$ ). Among the impurity scattering mechanisms, the potential associated with the charged impurities is sensitive to the electron-electron interactions. Typically the charged-impurity scattering potential is a screened Coulomb potential with a screening length determined by the Bloch-electron wave functions and the scattering matrix elements. Since an additional  $c$ -axis periodicity due to the antiferromagnetic ordering at  $T < T_{cl}$  gives rise to a zone-folding effect on the  $c$ -axis energy dispersion relation, both the scattering matrix elements and the electron density of states are modified. Therefore a change of resistivity is expected for both the in-plane ( $\rho_a$ ) and  $c$ -axis ( $\rho_c$ ) components of the resistivity. An increase in resistivity (for both  $\rho_a$  and  $\rho_c$  components) in the antiferromagnetic phase can be expected by the following simple argument. The Coulomb potential of the charged impurities becomes more correlated to the conduction electrons due to the additional  $c$ -axis periodicity introduced by the interplanar antiferromagnetic ordering. Thus the charged-impurity Coulomb potential becomes less screened, and the effective range of the potential is larger in the antiferromagnetic phase, thereby imposing larger scattering effects on the conduction electrons. Detailed calculations considering the modifications of the scattering matrix elements, the screening length, and the enhanced resistivity are given in Ref. 30, where it is shown that the essential condition for the Fermi-surface modification effect is that the dispersion along  $k_z$  cannot be neglected in writing the energy dispersion relation for

the  $\pi$  electrons,

$$E(\mathbf{k}) = E_a(\mathbf{k}_a) + E_z(k_z). \quad (14)$$

### D. Magnetic-field dependence

We begin with the discussion of the simpler case of the magnetoresistance measurements on stage-2  $\text{CoCl}_2$  GIC's [Fig. 3(b)]. For a magnetic system in the paramagnetic state, the presence of an external magnetic field gives rise to quantized spin states for the localized magnetic moments. The expectation values of any spin-related quantities for a paramagnetic system in a magnetic field should be calculated by summing over all the quantized spin states. In contrast, if a magnetic system is in a magnetically ordered phase below the magnetic phase-transition temperature, the spin configurations are primarily determined by the spin-exchange interactions, and the presence of a small external magnetic field does not have an important effect on the spin states. However, thermal agitations result in a deviation of the spins from their ideal ordered phase.

It should be emphasized that the magnetic field considered in the paramagnetic phase is the external field, while that in the magnetically ordered phase is the total magnetic field, which is the sum of the applied field and the internal exchange field (where the paramagnetic phase is defined by the absence of interlayer antiferromagnetic spin correlations). We show later that the observed  $T$  and  $H$  dependences are consistent, with spin-disorder scattering being the dominant magnetic scattering mechanism in stage-2  $\text{CoCl}_2$  GIC's.

If we neglect the scattering due to the second term in the curly braces of Eq. (8) and define  $S$  as the effective spin operator which is obtained from both the crystal-field (for Co,  $|S| = \frac{1}{2}$ ) and the trigonal-distortion corrections,<sup>39,40</sup> the resistivity in the paramagnetic phase is proportional to

$$\rho_{\text{para}} \propto S(S+1) - SB_S(x), \quad (15)$$

where  $B_S(x)$  is the Brillouin function,  $x \equiv [g^* \mu_B SH / k_B(T - \Theta)]$ , and since  $\Theta < 1$  K, it can be neglected in the  $T$  range of interest. It should be noted that Eq. (15) recovers the expression in Eq. (1). These simplified calculations yield results [Eq. (15)] which are consistent with those obtained by Yosida,<sup>41</sup> who employed a more complicated approach. Since  $B_S(x) \propto x$  for  $x \ll 1$ , and  $B_S(x) \rightarrow 1$  for  $x \gg 1$ , the  $H$  dependence of the resistivity contribution from spin-disorder scattering has an approximately linear negative slope ( $\partial \rho_{\text{spin}} / \partial H$ ) for small fields and approaches a constant value at high fields. A theoretical fit based on the above discussion and using Eq. (15) to fit the trace  $E$  in Fig. 3(b) is shown in Fig. 5, where the quantity  $[\rho(H, T > T_{cl}) / \rho(0, T)]$  is plotted as a function of magnetic field, and is compared to the theoretical curves

$$\{1 - [SB_S(x) / S(S+1)] \text{ versus } H\}$$

with  $g^*$  as the adjustable parameter and  $S = \frac{1}{2}$ . The best fit in Fig. 5 provides an effective  $g$  value of  $g^* \approx 5$ , in good



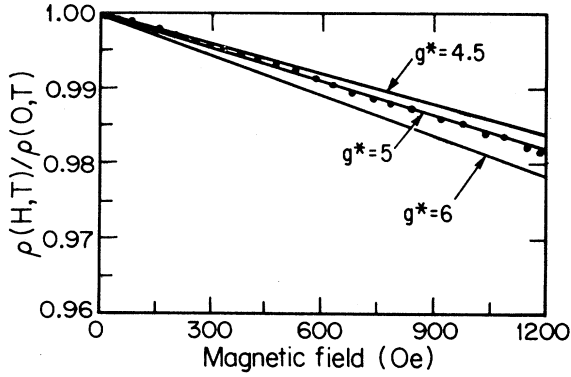


FIG. 5. Comparison of the experimental data and the theoretical calculations for the decrease of resistivity in a magnetic field due to spin-disorder scattering. The experimental data are taken from Fig. 3(b)  $E$  and are normalized to their zero-field resistivity values. The best fit for the experimental data yields  $g^* \approx 5$ , consistent with theory.<sup>39,40</sup>

agreement with the  $g^*$  value obtained from molecular-field theory<sup>39,40</sup> and the high-temperature magnetic-susceptibility measurements.<sup>35</sup>

In the magnetically ordered phase, we may replace  $x$  by

$$x' \equiv [g^* \mu_B S H_{\text{eff}} / k_B (T - \Theta)],$$

and  $H$  by  $H_{\text{eff}} \equiv H_E + H$ , where  $H_E$  is the internal exchange field of spins in the magnetically ordered phase. For the stage-2  $\text{CoCl}_2$  GIC, the Curie-Weiss temperature is very small ( $\Theta < 1$  K) and can be neglected. Therefore, the spin-disorder scattering below  $T_{cl}$  gives rise to a resistivity with the functional form

$$\rho_{\text{spin}}(H, T) = \rho(0) \left[ 1 + \frac{1}{S} \left\{ 1 - \frac{M_S(H_{\text{eff}}, T)}{M_0} \right\} \right], \quad (16)$$

where  $\rho(0)$  and  $M_0 = N_S g^* \mu_B S$  are independent of  $H$  and  $T$  and  $M_S(H_{\text{eff}}, T) = N_S g^* \mu_B S B_S(x')$ . For  $T \ll T_{cl}$ , since  $M_S(H_{\text{eff}}, T) \approx M_0$ , the resistivity due to the spin-order scattering becomes temperature independent, consistent with the nearly perfect magnetic ordering (e.g., antiferromagnetically ordered ferromagnetic sheets of spins). On the other hand, for  $T \rightarrow T_{cl}$ , then

$$M_S(H_{\text{eff}}, T \rightarrow T_{cl}^-) \rightarrow M_0 B_S(x),$$

and therefore Eq. (16) recovers the typical spin-disorder scattering term in the paramagnetic phase [Eq. (15)].

Because of the sharp decrease of  $M_S(T)$  as  $T \rightarrow T_{cl}$  from below, the negative magnetoresistance resulting from spin-disorder scattering has the most significant effect near  $T_{cl}$ , consistent with our experimental data [Figs. 1(b) and 2(b)]. The consistency between the observed temperature and magnetic-field effects supports the spin-disorder scattering mechanism proposed for stage-2  $\text{CoCl}_2$  GIC's.

long-range antiferromagnetic ordering below  $T_{cl}$  results in an additional scattering effect. As the external magnetic field in the basal plane is increased above  $H_{c2}$  (i.e.,  $H > H_{c2} \propto J'$ , where  $J'$  is the interplanar antiferromagnet-

ic coupling energy), the superspins on all the magnetic planes become aligned along the magnetic field, and the splitting in the  $E_z(k_z)$  dispersion relation disappears. Thus, a decrease in the resistivity is expected for  $H > H_{c2}$ , as is observed experimentally in Fig. 3(a).

For  $T \ll T_{cl}$  the critical magnetic field  $H_{c2}$  and the interplanar antiferromagnetic coupling constant ( $J'$ ) are related by

$$J' \approx \frac{g^* \mu_B H_{c2}}{S z'} \quad (17)$$

Inserting the values  $H_{c2}(T = 4.2 \text{ K}) \approx 330$  Oe,  $g^* \approx 5$ ,  $S = \frac{1}{2}$ , and  $z' = 6$  into Eq. (17), we obtain  $J' \approx 0.04$  K, consistent with the Monte Carlo calculation for the stage-1  $\text{CoCl}_2$  GIC's.<sup>35</sup> We make the following argument to explain the magnetoresistance measurements on stage-1  $\text{CoCl}_2$  GIC's shown in Fig. 3(a). The  $c$ -axis energy dispersion relation in the antiferromagnetic phase is modified relative to that of the paramagnetic phase by introducing an energy gap  $2\Delta$  at  $|k_z| = \pi/2I_c$ , where  $\Delta$  satisfies the condition<sup>30</sup>

$$\Delta = J_{\pi-d} \frac{N_s}{N_0} \left( \frac{1}{2} |\langle \mathbf{S}_a \rangle - \langle \mathbf{S}_b \rangle| \right), \quad (18)$$

in which  $N_s$  is the number of  $\text{Co}^{2+}$  ions per unit volume, and  $\langle \mathbf{S}_a \rangle$  and  $\langle \mathbf{S}_b \rangle$  are the thermodynamic averages of the spin angular momentum in magnetic sublattices  $a$  and  $b$ . We further observe that  $\langle \mathbf{S}_a \rangle$  and  $\langle \mathbf{S}_b \rangle$  are opposite in sign for  $T < T_{cl}$  and  $H < H_{c2}$ . Once the external magnetic field exceeds the exchange coupling  $J'$ , the difference between the sublattice magnetization  $|\langle \mathbf{S}_a \rangle - \langle \mathbf{S}_b \rangle|$  decreases with increasing magnetic field. Therefore the energy gap  $\Delta$  in the  $c$ -axis dispersion relation begins to decrease with increasing magnetic field for applied fields  $H > H_{c2}$ , and becomes zero if  $H \gg H_{c2}$ . Since the decrease in the resistivity of the stage-1 compound in a magnetic field is directly related to the decreasing energy gap  $\Delta$ , the field dependence of  $\rho(H, T)$  in Fig. 3(a) decreases with  $H$  for  $H > H_{c2}$ . It should be noted that the decrease of resistivity is not saturated even at the highest available magnetic field (1.2 kOe), indicating that the antiferromagnetically coupled superspins are not completely aligned. This observation is consistent with the latest magnetostriction experiments on stage-1  $\text{CoCl}_2$  GIC's,<sup>26</sup> in which other magnetic phase transitions are indicated for  $H > 1$  kOe. In the case of stage-2  $\text{CoCl}_2$  GIC's, no critical field (analogous to  $H_{c2}$ ) was observed in the resistivity measurements within the experimental resolution of  $\pm 10$  Oe [Fig. 3(b)], indicating either a much smaller interplanar antiferromagnetic coupling constant ( $J' < 10^{-3}$  K), or a short-range interplanar antiferromagnetic coupling which suppresses the Fermi-surface modification effect. The estimate of the upper limit of  $J'$  for stage-2  $\text{CoCl}_2$  GIC's from the preceding discussion is consistent with estimates of  $J'$  from magnetic susceptibili-

ty<sup>35,36</sup> and neutron scattering measurements,<sup>4,5,31</sup> which give  $J' \approx 10^{-3} \sim 10^{-4}$  K.

## V. MECHANISM FOR THE INTERPLANAR MAGNETIC COUPLING IN MAGNETIC GIC'S

In the preceding section, we examined the magnetic scattering effects through the  $\pi$ - $d$  exchange interaction. This concept naturally introduces a possible exchange interaction between  $\text{Co}^{2+}$  ions through their coupling with  $\pi$  electrons. In this section we consider three mechanisms for coupling the interplanar magnetic cobalt spins in an acceptor intercalation compound: the RKKY interaction, the dipole-dipole interaction, and the superexchange interaction. The exchange energies for each of these mechanisms is estimated using appropriate models. Since the acceptor-type magnetic GIC's consist of layered insu-

lators (metal chlorides) and metals (graphite), the interplanar magnetic exchange interactions are much more complicated than the typical superexchange interaction in insulators and the RKKY interaction in metals.

### A. RKKY interaction in acceptor-type magnetic GIC's

In this section, we propose a modified RKKY calculation applicable for magnetic GIC systems and we estimate the interplanar RKKY interaction energy for  $\text{CoCl}_2$  GIC's. The RKKY interaction for these highly anisotropic magnetic superlattices is shown to be negligibly small, in contrast to that in the dilute magnetic alloys.<sup>11-13</sup>

The RKKY interaction between magnetic species at  $\mathbf{R}_i$  and  $\mathbf{R}_j$  via the double scattering of an electron ( $\mathbf{k} \rightarrow \mathbf{k}' \rightarrow \mathbf{k}$ ) at  $T=0$  is<sup>11,12,13</sup>

$$\begin{aligned} \mathcal{H}_{\text{ex}}(\mathbf{R}_{ij}) &= -\text{Tr}\{(\boldsymbol{\sigma} \cdot \mathbf{S}_i)(\boldsymbol{\sigma} \cdot \mathbf{S}_j)\} \left[ \int_0^{k_F} d^3k \frac{\Omega_0}{(2\pi)^3} \int_{k_F}^{\infty} d^3k' \frac{\Omega_0}{(2\pi)^3} \frac{J_{\text{ex}}(\mathbf{k}, \mathbf{k}') J_{\text{ex}}(\mathbf{k}', \mathbf{k}) e^{i(\mathbf{k}-\mathbf{k}') \cdot \mathbf{R}_{ij}}}{E(\mathbf{k}') - E(\mathbf{k})} + \text{c.c.} \right] \\ &\equiv J(\mathbf{R}_{ij}) \{\mathbf{S}_i \cdot \mathbf{S}_j\}, \end{aligned} \quad (19)$$

where  $\mathbf{R}_{ij} = \mathbf{R}_i - \mathbf{R}_j$ , and  $k_F$  is the wave vector at the Fermi level, while  $\Omega_0$  denotes a unit volume, and  $J(\mathbf{R}_{ij})$  is defined as the RKKY exchange interaction energy between spin  $\mathbf{S}_i$  and spin  $\mathbf{S}_j$ ,

$$J(\mathbf{R}_{ij}) \equiv \left[ \frac{\text{Tr}[(\boldsymbol{\sigma} \cdot \mathbf{S}_i)(\boldsymbol{\sigma} \cdot \mathbf{S}_j)]}{(\mathbf{S}_i \cdot \mathbf{S}_j)} \right] I_1, \quad (20)$$

and  $I_1$  is an oscillatory function of  $R_{ij}$ .<sup>21</sup> Since the most important contribution to Eq. (19) comes from  $k \sim k' \sim k_F$ , the expression  $[J_{\text{ex}}(\mathbf{k}, \mathbf{k}') J_{\text{ex}}(\mathbf{k}', \mathbf{k})]$  may be approximated<sup>11</sup> by the constant  $|J_{\text{ex}}(k_F, k_F)|^2$ .

For an isotropic three-dimensional system,  $J(\mathbf{R}_{ij})$  is calculated in spherical coordinates to be<sup>11-13</sup>

$$\begin{aligned} J(\mathbf{R}_{ij}) &= \frac{\Omega_0^2 m_e^*}{4(2\pi)^3 \hbar^2} \frac{|J_{\text{ex}}|^2}{R_{ij}^4} [2k_F R_{ij} \cos(2k_F R_{ij}) \\ &\quad - \sin(2k_F R_{ij})], \end{aligned} \quad (21)$$

where the exchange constant  $J(\mathbf{R}_{ij})$  oscillates between ferromagnetic and antiferromagnetic coupling, depending on the magnitude of  $2k_F R_{ij}$ . The divergence at  $2k_F R_{ij} \rightarrow 0$  can be handled by including the  $k$  dependence of  $J_{\text{ex}}$ , as described in Refs. 12 and 13. In contrast, since GIC's form  $c$ -axis superlattices and the in-plane  $\pi$ -electron dispersion relation in GIC's is approximately linear<sup>42</sup> in  $k_a$  [i.e.,  $E(\mathbf{k}_a) \approx \pm p_0 k_a$ ], it is convenient to calculate the RKKY exchange constant  $J(\mathbf{R}_{ij})$  in a cylindrical coordinate system because of the highly anisotropic Fermi surface of GIC's. Specifically, it is shown that for an isotropic in-plane dispersion relation the in-plane RKKY coupling between spins in the same basal plane becomes identically zero, because  $I_1$  in Eq. (20) is then

$$I_1 \propto \frac{1}{R_z^2} \sin^2(\pi R_z / I_c) \quad (22)$$

and

$$\sin^2(\pi R_z / I_c) \Big|_{R_z=0} = 0. \quad (23)$$

Moreover, the  $c$ -axis RKKY interaction between spins separated by  $nI_c$  (stage  $n=1, 2, \dots$ ) is also identically zero.<sup>21</sup>

Because of the small magnitude of the RKKY interaction for these quasi-two-dimensional systems,<sup>21</sup> we conclude that the RKKY interaction is not the dominant magnetic exchange mechanism for acceptor-type magnetic GIC's due to their large magnetic and electronic anisotropy. This is in contrast to the donor-type magnetic compound  $\text{C}_6\text{Eu}$ , which exhibits three-dimensional magnetic interactions and a much smaller electronic anisotropy. Therefore the RKKY interaction calculated for 3D systems is appropriate for  $\text{C}_6\text{Eu}$ , and is in fact the dominant magnetic exchange mechanism for the  $\text{C}_6\text{Eu}$  system.<sup>24</sup>

### B. Dipole-dipole interaction

It is natural to consider the dipole-dipole interaction for any magnetic system, since any localized magnetic moment generates a dipolar magnetic field, which directly interacts with other localized magnetic moments. The dipole-dipole energy ( $E_{d-d}$ ) for one spin  $\mathbf{S}_1$  at the origin interacting with all other spins  $\mathbf{S}_i$  can be written as

$$E_{d-d} = (g^* \mu_B)^2 \left[ \sum_i^{z_1} \frac{\mathbf{S}_1 \cdot \mathbf{S}_{2i}}{R_i^3} - \frac{3(\mathbf{S}_1 \cdot \mathbf{R}_i)(\mathbf{S}_{2i} \cdot \mathbf{R}_i)}{R_i^5} \right] + \left[ \sum_j^{z_2} \frac{\mathbf{S}_1 \cdot \mathbf{S}_{2j}}{R_j^3} - \frac{3(\mathbf{S}_1 \cdot \mathbf{R}_j)(\mathbf{S}_{2j} \cdot \mathbf{R}_j)}{R_j^5} \right] + \dots$$

$$\equiv J_{d-d}^{(1)} \left[ \sum_i^{z_1} \mathbf{S}_1 \cdot \mathbf{S}_{2i} \right] + J_{d-d}^{(2)} \left[ \sum_j^{z_2} \mathbf{S}_1 \cdot \mathbf{S}_{2j} \right] + \dots, \quad (24)$$

where  $g^*$  is the effective  $g$  value,  $R_i$  is the distance between  $\mathbf{S}_1$  and its nearest-neighbor spins,  $z_1$  is the number of the nearest spins,  $J_{d-d}^{(1)}$  denotes the corresponding dipole-dipole coupling constant for the nearest neighbors;  $R_j$  is the distance between  $\mathbf{S}_1$  and its next-nearest-neighbor spins,  $z_2$  is the number of the next-nearest spins,  $J_{d-d}^{(2)}$  denotes the corresponding dipole-dipole coupling constant for the next nearest neighbors, etc.<sup>43</sup>

Since the magnetic coupling constants in a magnetic Hamiltonian are defined as the coupling energy between each pair of spins, we consider the interaction energies for a pair of nearest spins when making a comparison between the nearest-neighbor coupling constants for various mechanisms. In this context, we estimate the interplanar dipole-dipole coupling constant  $J'_{d-d}$  according to Eq. (24), which yields the following formula:

$$E'_{d-d} = J'_{d-d} \sum_{i=1}^{z'} \mathbf{S}_1 \cdot \mathbf{S}_{2i}, \quad (25)$$

$$= J'_{d-d} (z' \mathbf{S}_1 \cdot \mathbf{S}_2), \quad (26)$$

where  $E'_{d-d}$  denotes the dipole field energy associated with the coupling between spin  $\mathbf{S}_1$  and its nearest-neighbor spins in the adjacent layers,  $J'_{d-d}$  denotes the corresponding pair coupling constant,  $z'$  is the number of nearest neighbors in the adjacent layers, and Eq. (25) can be simplified to Eq. (26) provided that the spins in each layer are all of the same kind. We estimate  $J'_{d-d}$  as the upper bound for the dipole-dipole interaction between each pair of spins because

$$E_{d-d} \equiv \langle J'_{d-d} \rangle \sum_i^N \mathbf{S}_1 \cdot \mathbf{S}_{2i} \leq J'_{d-d} N \langle S_1^2 \rangle, \quad (27)$$

where  $\langle J'_{d-d} \rangle$  is the average pair interaction and  $N$  is the total number of  $\text{Co}^{2+}$  ions.

In carrying out the sum over nearest neighbors explicitly, it is found<sup>21</sup> that the interplanar dipole-dipole interaction in  $\text{CoCl}_2$  GIC's gives rise to antiferromagnetic coupling as for the case of pristine  $\text{CoCl}_2$ . Using the interplanar effective  $g$  factor (3.38) for pristine  $\text{CoCl}_2$  and the effective spin operators  $\mathbf{S}$  including the crystal-field and trigonal-distortion corrections,<sup>39,40</sup> we calculated the coupling constants  $J'_{d-d} \sim 7 \times 10^{-3}$  K for stage-1 and  $\sim 3 \times 10^{-3}$  K for stage-2  $\text{CoCl}_2$  GIC's, respectively. It should be noted that these numbers are slightly overestimated, since the interplanar  $g$  values in GIC's should be slightly reduced and higher-order terms in the sum in Eq. (24) should be considered. Though the estimate for  $E_{d-d}$  is only approximate, we can conclude that in stage-1

$\text{CoCl}_2$  GIC's, the dipole-dipole interaction energy is too small to account for the interplanar antiferromagnetic coupling of  $10^{-1}$  to  $10^{-2}$  K observed from the experiments.

### C. Superexchange interaction

The superexchange interaction between two magnetic ions through diamagnetic molecules in magnetic insulators can be simplified as a consequence of the interplay between two major types of interactions: the potential exchange interaction, and the kinetic exchange interaction.<sup>44,45</sup> The potential exchange interaction is an interaction energy between the orthogonal orbitals of the magnetic ions, which is basically the Coulomb exchange interaction under the Hartree-Fock approximation, and is in general ferromagnetic, while the kinetic exchange interaction is determined by the hopping effect between the nonorthogonal orbitals of the magnetic ions and the intervening anions. The hopping effect results in two important consequences: One is the pairing of electrons between one set of magnetic  $d$ -electron orbitals and the  $s, p$  orbitals of the anions, thereby forming a partially covalent bonding and lowering the total energy of the complex; the other is the formation of magnetic coupling between the other set of unpaired anion  $p$  orbitals and the magnetic  $d$  electrons. [This concept is schematically illustrated in Fig. 6(a) for pristine  $\text{CoCl}_2$  GIC's.] In this context, the sign of the kinetic exchange energy is determined by both types of interacting orbitals as well as the

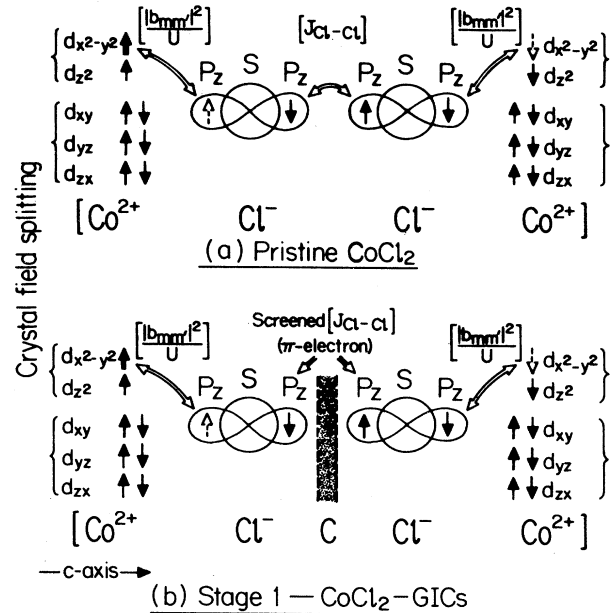


FIG. 6. Models for the interplanar superexchange coupling in (a) pristine  $\text{CoCl}_2$  and (b)  $\text{CoCl}_2$  GIC's. We have simplified the  $c$ -axis stacking in these figures, since in the actual  $\text{CoCl}_2$  GIC's, the bonding angles between  $\text{Co}^{2+}/\text{Cl}^-/\text{Cl}^-/\text{Co}^{2+}$  are not exactly  $180^\circ$  (i.e., these atoms do not lie along a straight line).

bonding angles between the cations and anions. The resulting sign of the superexchange interaction in the magnetic insulators is determined by the sum of the potential exchange and kinetic exchange contributions. The general rules for determining the sign of superexchange interactions are well established by Goodenough and Kanamori.<sup>44,46,47</sup>

The superexchange interactions of  $\text{CoCl}_2$  as well as other transition-metal chlorides are discussed elsewhere<sup>21</sup> using the Goodenough-Kanamori rules.<sup>44-47</sup> The model for the interplanar superexchange interaction in pristine  $\text{CoCl}_2$  is shown in Fig. 6(a). It should be noted that in the pristine transition-metal chlorides, there are two layers of  $\text{Cl}^-$  ions between consecutive cation layers. Therefore the superexchange interactions have to go through modified electron wave functions between  $\text{Co}^{2+}$  and  $\text{Cl}^-$  as well as through  $\text{Cl}^-$ - $\text{Cl}^-$  exchange interactions. We define the exchange energy between  $\text{Cl}^-$ - $\text{Cl}^-$  ions as  $J_{\text{Cl-Cl}}(R_{12})$ , where  $R_{12}$  is the separation between nearest  $\text{Cl}^-$  layers. Since  $\text{Cl}^-$ - $\text{Cl}^-$  can form a covalent  $p_\sigma$  bond through the Coulomb exchange interaction, an antiferromagnetic coupling for  $J_{\text{Cl-Cl}}$  is expected to lower the energy of the system. We may therefore write the total interplanar  $\text{Co}^{2+}$ - $\text{Co}^{2+}$  superexchange (sx) interaction energy as

$$\mathcal{H} \equiv J'_{\text{sx}} (\mathbf{S}_a \cdot \mathbf{S}_b), \quad (28)$$

$$J'_{\text{sx}} \approx \left( \frac{b_t}{U} \right)^4 J_{\text{Cl-Cl}}(R_{12}),$$

where  $b_t$  is the transfer energy which gives rise to an electron transfer from a  $\text{Cl}^-$  anion to a neighboring  $\text{Co}^{2+}$  cation. The quantity  $U$  is the Coulomb repulsion energy of two  $d$  electrons in the same orbitals,<sup>48</sup> and both  $b_t^4/U^4$  and  $J_{\text{Cl-Cl}}(R_{12})$  are positive in sign.

Since the kinetic exchange ( $b_t^4/U^4$ ) in pristine  $\text{CoCl}_2$  is not significantly changed after intercalation [Figs. 6(a) and 6(b)], while the Coulomb type exchange energy ( $J_{\text{Cl-Cl}}$ ) between  $\text{Cl}^-$ - $\text{Cl}^-$  is strongly weakened by the insertion of sheets of  $\pi$  conduction electrons after intercalation [Fig. 6(b)], it is suggested that the interplanar antiferromagnetic coupling in  $\text{CoCl}_2$  GIC's is reduced in a way resembling the screened Coulomb potential for charged impurities in a free-electron gas. In other words, since the effective exchange interaction between  $\text{Cl}^-$ - $\text{Cl}^-$  layers is greatly reduced as compared to that in pristine  $\text{CoCl}_2$ , we may estimate the stage dependence of the interplanar superexchange interaction  $J'_{\text{sx}}$  for  $\text{CoCl}_2$  GIC's according to Eq. (28), provided that the screening constant  $\lambda_n$  is known:

$$\frac{\{J'_{\text{sx}}\}_{\text{stage-(n+1)}}}{\{J'_{\text{sx}}\}_{\text{stage-n}}} \approx \frac{J_{\text{Cl-Cl}}(R_{n+1})}{J_{\text{Cl-Cl}}(R_n)} \approx e^{-[(n+1)\lambda_{n+1} - n\lambda_n]\bar{c}_0}, \quad (29)$$

where  $R_n = R_{12} + n\bar{c}_0$ , and  $R_{12}$  is the separation between  $\text{Cl}^-$ - $\text{Cl}^-$  layers in pristine  $\text{CoCl}_2$ , while  $\lambda_n$  is the screening constant for a stage- $n$  sample and  $\bar{c}_0$  is the interplanar

distance between graphite layers (3.35 Å). Typically  $\lambda_n \sim 10^8 \text{ cm}^{-1}$  for  $n=1$ , and  $\lambda_n$  decreases with increasing stage index  $n$ . Using the known interplanar superexchange constant  $J'_{\text{sx}} = 2.16 \text{ K}$  for pristine  $\text{CoCl}_2$  and Eq. values for various stages can be estimated. We thus obtain the estimates  $J'_{\text{sx}} = 10^{-1} \sim 10^{-2} \text{ K}$  for stage-1  $\text{CoCl}_2$  GIC's, and  $J'_{\text{sx}} \sim 10^{-3} \text{ K}$  for stage-2. It should be noted that the estimated value for the stage-1 compound is consistent with the transport data discussed in Secs. III and IV, which yields  $J'_{\text{stage-1}} \approx 0.04 \text{ K}$ , and the estimated value for the stage-2 compound is also consistent with the magnetic susceptibility<sup>35,36</sup> and neutron scattering<sup>31</sup> experiments, which give  $J'_{\text{stage-2}} \approx 10^{-3} \text{ K}$ . The model for the interplanar antiferromagnetic coupling between  $\text{Co}^{2+}$  ions for  $\text{CoCl}_2$  GIC's is depicted in Fig. 6(b). More details on the calculation of  $J'_{\text{sx}}$  based on the microscopic picture of wave-function mixing and electron transfer are given elsewhere.<sup>30</sup>

After estimating all the interplanar coupling constants for the superexchange, dipole-dipole, and RKKY interactions, we obtain a net interplanar antiferromagnetic coupling for  $\text{CoCl}_2$  GIC's, and the magnitude is approximately  $10^{-1} \sim 10^{-2} \text{ K}$  for stage-1 and  $\sim 10^{-3} \text{ K}$  for stage-2 compounds, consistent with our transport measurements and with other experiments.<sup>31,35</sup> We find that the dominant  $c$ -axis magnetic exchange mechanism for pristine  $\text{CoCl}_2$  and stage-1  $\text{CoCl}_2$  GIC's is the superexchange interaction, while in the case of stage-2  $\text{CoCl}_2$  GIC's, both the dipole-dipole and the superexchange interactions are equally important. In the case of higher-stage  $\text{CoCl}_2$  GIC's, ( $n \geq 3$ ), the dipole-dipole interaction dominates because of the rapid decrease of the superexchange interaction with increasing stage index. A schematic illustration for the superexchange and dipole-dipole exchange coupling constants versus stage index is shown in Fig. 7. It should be emphasized that our proposed models for the  $c$ -axis magnetic exchange mecha-

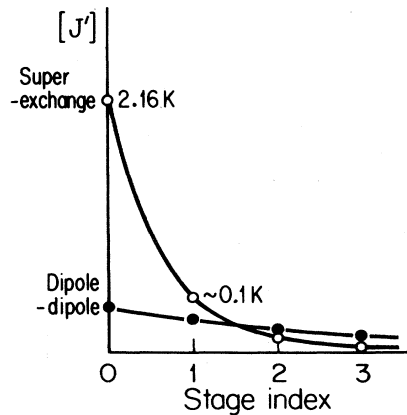


FIG. 7. Schematic comparison of the  $c$ -axis superexchange and dipole-dipole exchange constants vs stage index. Both the superexchange and the dipole-dipole interactions provide  $c$ -axis antiferromagnetic coupling for the  $\text{CoCl}_2$  GIC's.

nisms are generally applicable to all the magnetic transition-metal chloride acceptor GIC's.

## VI. DISCUSSION

In this section, we compare the  $\text{CoCl}_2$  GIC's to other magnetic systems and discuss the similarities and differences. The low-temperature anomalies in the transport measurements on  $\text{CoCl}_2$  GIC's were already shown in the previous sections to be closely related to the magnetic ordering. It is significant that the spin-disorder scattering effect and the short-range coupling effect, which are discussed for  $T$  slightly higher than the Néel temperature ( $T_{cl}$ ), are typical properties of magnetic metals, as is also seen in typical magnetic alloys. In contrast, the anomalies observed in stage-1  $\text{CoCl}_2$  GIC's due to the Fermi-surface modification are an unusual consequence of the highly anisotropic electronic and magnetic properties of this compound in contrast to the isotropic magnetic and electronic distributions in magnetic alloys. We expect similar effects to be observed in other layered magnetic metals with quasi-2D electronic properties, high  $XY$  spatial anisotropy, and a long-range  $c$ -axis antiferromagnetic correlation length.

The transport properties of the donor-type magnetic GIC's ( $\text{C}_6\text{Eu}$ ) show strong magnetic scattering effects<sup>23</sup> because of the direct interaction between conduction  $\pi$  electrons and the  $f$  electrons of Eu. The magnetic exchange coupling in  $\text{C}_6\text{Eu}$  is dominated by the RKKY interaction,<sup>24</sup> which is in contrast to the much more complicated coupling mechanisms in acceptor-type magnetic GIC's. The complicated mechanisms in the latter case are due to the presence of diamagnetic  $\text{Cl}^-$ -anion sheets sandwiched between magnetic  $\text{Co}^{2+}$  cations and the graphite conduction  $\pi$  electrons. Note that  $\text{C}_6\text{Eu}$  is a 3D-Heisenberg system, which has an antiferromagnetic nearest-neighbor in-plane coupling and ferromagnetic interplanar coupling. The type of scattering associated with the Fermi-surface modification in the stage-1  $\text{CoCl}_2$  GIC does not exist in  $\text{C}_6\text{Eu}$  because the interplanar magnetic superlattices have the same periodicity as the structural superlattices. On the other hand, although the magnetic phase diagram of  $\text{C}_6\text{Eu}$  is much more complicated compared to that of  $\text{CoCl}_2$  GIC's, the spin-disorder scattering effect was also observed in both  $H$  and  $T$ -dependent resistivity measurements in  $\text{C}_6\text{Eu}$ ,<sup>22-24</sup> consistent with our theoretical modeling. We also note that for other acceptor magnetic GIC's such as  $\text{MnCl}_2$  GIC's, which have in-plane nearest-neighbor antiferromagnetic coupling and interplanar ferromagnetic coupling, spin-disorder scattering was also observed.<sup>25</sup> The spin-disorder scattering effect is generally much smaller for acceptor-type magnetic GIC's than that for  $\text{C}_6\text{Eu}$  because of the large separation between the spins and the  $\pi$  electrons.

## VII. SUMMARY

The transport properties of stage-1 and stage-2  $\text{CoCl}_2$  GIC's were studied as a function of temperature ( $T$ ) and magnetic field ( $H$ ). Anomalies in the resistivity are attributed to various magnetic scattering effects associated with the magnetic ordering in the  $\text{CoCl}_2$  GIC's. Two

scattering effects based on the concept of  $\pi$ - $d$  electron exchange coupling are proposed to explain the experimental data. The coupling constant  $J_{\pi-d}$  was estimated from the experimental data.

The spin-disorder scattering effect was found to be the dominant magnetic scattering effect in stage-2  $\text{CoCl}_2$  GIC's for temperatures near  $T_{cl}$ , which is clearly illustrated by the consistency between the temperature and the magnetic-field dependence. However, in stage-1  $\text{CoCl}_2$  GIC's, an additional scattering effect associated with the long-range interplanar antiferromagnetic ordering is found to be about one order of magnitude larger than the spin-disorder scattering for  $T < T_N$ . Such a scattering effect is a special feature of the stage-1  $\text{CoCl}_2$  GIC's because of the highly anisotropic electronic and magnetic properties. This is in contrast to the spin-disorder scattering and the short-range spin-correlation effects, which are typical of magnetic metals and are observed in both stage-1 and stage-2  $\text{CoCl}_2$  GIC's.

The temperature dependence of the transport anomalies is qualitatively related to the magnetic properties of  $\text{CoCl}_2$  GIC's in terms of universal exponents. The magnetic-field dependence is examined by theoretical modeling, and its consistency with the temperature dependence supports the proposed two magnetic scattering effects in  $\text{CoCl}_2$  GIC's. The interplanar antiferromagnetic coupling constant  $J'$  for the stage-1 compound is estimated from the measured critical magnetic field. The physical pictures of how the two antiferromagnetic sublattices behave in an external magnetic field are also discussed.

The magnetic exchange couplings in the acceptor-type magnetic GIC's are much more complicated than the RKKY interaction in magnetic alloys and the superexchange interaction in magnetic insulators. The magnitude of the RKKY interaction in GIC acceptor compounds is shown to be negligibly small due to the large magnetic and electronic anisotropy. The interplanar superexchange couplings in GIC's are treated using a semiempirical method. We conclude that the interplanar antiferromagnetic coupling in stage-1  $\text{CoCl}_2$  GIC's is dominated by the superexchange interaction, and the dipole-dipole interaction is comparable to the superexchange interaction in stage-2  $\text{CoCl}_2$  GIC's. The interplanar antiferromagnetic coupling in higher stages ( $n \geq 3$ ) is dominated by the dipole-dipole interaction because of the relatively slower power-law decrease with distance as compared to the exponential decrease of the superexchange interaction.

## ACKNOWLEDGMENTS

The authors would like to acknowledge Dr. S.-T. Chen for useful discussions and for his help with sample preparation. This research was supported by the Air Force Office of Scientific Research Contract No. F49620-83-C-0011 during the early phases of this work and by National Science Foundation (NSF) Grant No. DMR83-10482 for the later phases. This research is in partial fulfillment of the requirements of the Ph.D. degree of N.-C.Y. in Physics at the Massachusetts Institute of Technology.

- \*Now at the IBM Thomas J. Watson Research Center (P.O. Box 218), Yorktown Heights, NY 10598.
- †Now at Nihon University, College of Pharmacy 7-chome 7-1, Narashino-dai, Funabashi, Chiba, 274 Japan.
- <sup>1</sup>M. T. Hutchings, *J. Phys. C* **6**, 3143 (1973).
- <sup>2</sup>J. M. Kosterlitz and D. J. Thouless, *J. Phys. C* **6**, 1181 (1973).
- <sup>3</sup>M. Suzuki, P. C. Chow, and H. Zabel, *Phys. Rev. B* **32**, 6800 (1985).
- <sup>4</sup>D. G. Wiesler, M. Suzuki, H. Zabel, S. M. Shapiro, and R. M. Nicklow, *Physica* **136B**, 22 (1986).
- <sup>5</sup>H. Zabel and S. M. Shapiro, *Phys. Rev. B* **36**, 7292 (1987).
- <sup>6</sup>J. T. Nicholls, Y. Shapira, E. J. McNiff, Jr., and G. Dresselhaus, *Synth. Met.* **23**, 231 (1988).
- <sup>7</sup>M. Elahy and G. Dresselhaus, *Phys. Rev. B* **30**, 7225 (1984).
- <sup>8</sup>S. T. Chen, K. Y. Szeto, M. Elahy, and G. Dresselhaus, *J. Chim. Phys.* **81**, 863 (1984).
- <sup>9</sup>K. Koga and M. Suzuki, *J. Phys. Soc. Jpn.* **53**, 786 (1984).
- <sup>10</sup>M. Suzuki, I. Oguro, and Y. Jinzaki, *J. Phys. C* **17**, L575 (1984).
- <sup>11</sup>M. A. Ruderman and C. Kittel, *Phys. Rev.* **96**, 99 (1954).
- <sup>12</sup>T. Kasuya, *Prog. Theor. Phys.* **16**, 45 (1956).
- <sup>13</sup>K. Yosida, *Phys. Rev.* **106**, 893 (1957).
- <sup>14</sup>M. Suzuki, H. Ikeda, and Y. Endoh, *Synth. Met.* **8**, 43 (1983).
- <sup>15</sup>H. C. Montgomery, *J. Appl. Phys.* **42**, 2971 (1971).
- <sup>16</sup>M. S. Dresselhaus and G. Dresselhaus, *Adv. Phys.* **30**, 139 (1981).
- <sup>17</sup>E. McRae, D. Billaud, J. F. Marêché, and A. Hérold, *Physica* **99B**, 489 (1980).
- <sup>18</sup>H. Suematsu, K. Higuchi, and S. Tanuma, *J. Phys. Soc. Jpn.* **48**, 1541 (1980).
- <sup>19</sup>K. Sugihara, in *Extended Abstracts of the Symposium on Intercalated Graphite at the Materials Research Society Meeting, Boston, 1984*, edited by P. C. Eklund, M. S. Dresselhaus, and G. Dresselhaus (Materials Research Society, Pittsburgh, PA, 1984), p. 60.
- <sup>20</sup>H. Kamimura, K. Nakao, T. Ohno, and T. Inoshita, *Physica* **99B**, 401 (1980).
- <sup>21</sup>N. C. Yeh, Ph.D. thesis, Massachusetts Institute of Technology, 1988.
- <sup>22</sup>H. Suematsu, H. Minemoto, K. Ohmatsu, Y. Yosida, S. T. Chen, G. Dresselhaus, and M. S. Dresselhaus, *Synth. Met.* **12**, 377 (1985).
- <sup>23</sup>S. T. Chen, G. Dresselhaus, M. S. Dresselhaus, H. Suematsu, H. Minemoto, K. Ohmatsu, and Y. Yosida, *Phys. Rev. B* **34**, 423 (1986).
- <sup>24</sup>K. Sugihara, S. T. Chen, and G. Dresselhaus, *Synth. Met.* **12**, 383 (1985).
- <sup>25</sup>N. C. Yeh, T. Enoki, L. Salamanca-Riba, and G. Dresselhaus, in *Extended Abstracts of the 17th Biennial Conference on Carbon, University of Kentucky, 1985* (American Carbon Society, State College, PA, 1985), p. 194.
- <sup>26</sup>J. T. Nicholls, G. Dresselhaus, Y. Iye, and G. Miura, *Bull. Am. Phys. Soc.* **33**, 729 (1988).
- <sup>27</sup>G. Chouteau, L. Puech, and R. Yazami, in *International Colloquium on Layered Compounds, Pont-a-Mousson, 1988*, edited by D. Guérard and P. Lagrange (unpublished), p. 211.
- <sup>28</sup>M. E. Fisher and J. S. Langer, *Phys. Rev. Lett.* **20**, 665 (1968).
- <sup>29</sup>G. Chouteau, J. Schweizer, F. Tasset, and R. Yazami, *Synth. Met.* **23**, 249 (1988).
- <sup>30</sup>K. Sugihara, N. C. Yeh, M. S. Dresselhaus, and G. Dresselhaus, *Phys. Rev. B* **39**, 4577 (1988).
- <sup>31</sup>M. Suzuki, D. G. Wiesler, P. C. Chow, and H. Zabel, *J. Magn. Magn. Mater.* **54-57**, 1275 (1986).
- <sup>32</sup>H. Zabel, *Phys. Rev. Lett.* **12**, 225 (1986).
- <sup>33</sup>D. G. Wiesler, M. Suzuki, and H. Zabel, *Phys. Rev. B* **36**, 7051 (1987).
- <sup>34</sup>D. G. Wiesler and H. Zabel, *Phys. Rev. B* **36**, 7303 (1987).
- <sup>35</sup>S. T. Chen, Ph.D. thesis, Massachusetts Institute of Technology, 1985.
- <sup>36</sup>K. Y. Szeto, S. T. Chen, and G. Dresselhaus, *Phys. Rev. B* **32**, 4628 (1985).
- <sup>37</sup>R. M. White, in *Quantum Theory of Magnetism*, Vol. 32 of *Springer Series in Solid-State Sciences*, edited by M. Cardona, P. Fulde, and H. Queisser (Springer, New York, 1983).
- <sup>38</sup>S. Ma, in *Modern Theory of Critical Phenomena, Frontiers in Physics*, edited by D. Pines (Addison-Wesley, Reading, MA, 1976).
- <sup>39</sup>M. E. Lines, *Phys. Rev.* **131**, 540 (1963).
- <sup>40</sup>M. E. Lines, *Phys. Rev.* **131**, 546 (1963).
- <sup>41</sup>K. Yosida, *Phys. Rev.* **147**, 223 (1966).
- <sup>42</sup>J. Blinowski, H. H. Nguyen, C. Rigaux, J. P. Vieren, R. LeToullec, G. Furdin, A. Hérold, and J. Mélin, *J. Phys. (Paris)* **41**, 47 (1980).
- <sup>43</sup>H. Kornfeld, *Z. Phys.* **22**, 27 (1924).
- <sup>44</sup>J. B. Goodenough, *Magnetism and the Chemical Bond* (Wiley, New York, 1963).
- <sup>45</sup>P. W. Anderson, in *Solid State Physics*, edited by F. Seitz and D. Turnbull (Academic, New York, 1963), Vol. 14, pp. 99-214.
- <sup>46</sup>J. B. Goodenough, *Phys. Rev.* **100**, 564 (1955).
- <sup>47</sup>J. Kanamori, *J. Phys. Chem. Solids* **10**, 87 (1959).
- <sup>48</sup>P. W. Anderson, *Phys. Rev.* **79**, 350 (1950).